Published in Cretaceous Research 28, issue 4, 597-612, 2007
which should be used for any reference to this work

The Cenomanian/Turonian anoxic event at the Bonarelli Level in Italy and Spain: enhanced productivity and/or better preservation?

Haydon Mort [a,*], Olivier Jacquat [c], Thierry Adatte [a], Philip Steinmann [a], Karl Föllmi [a], Virginie Matera [a], Zsolt Berner [b], Doris Stüben [b]

[a] *Institut de Géologie, Emile Argand 11, 2007 Neuchâtel, Switzerland*
[b] *Institut für Mineralogie und Geochemie, Universität Karlsruhe, 76128 Karlsruhe, Germany*
[c] *Institute of Biogeochemistry and Pollutant Dynamics, Department of Environmental Sciences, ETH Zürich, Universitätstrasse 16, CH-8092 Zürich, Switzerland*

Abstract

The upper Cenomanian pelagic sediments of Furlo in the northern Apennines, Italy, are characterized by a 1.5-m-thick organic-rich stratigraphic horizon called the Bonarelli Level, which represents the second major oceanic anoxic event in the Cretaceous (OAE 2). The Bonarelli Level is depleted in carbonates and consists essentially of biogenic quartz, phyllosilicates, and organic matter, with values of TOC reaching 18%. The age of the Furlo section is constrained by correlating its $\delta^{13}C$ curve with that of the well-dated Pueblo (USA) and Eastbourne (UK) sections. The presence of all the planktonic foraminiferid zones and details of the OAE 2 $\delta^{13}C$ excursion indicates a relatively continuous but reduced sedimentation rate across the Cenomanian/Turonian (C/T) boundary. Sediment and TOC mass accumulation rates have been calculated and suggest a sedimentation break in the upper Bonarelli Level. This may be an artifact of the diachronous FAD of the planktonic foraminiferid *Helvetoglobotruncana helvetica* and suggests that in some sections the $\delta^{13}C$ curve may provide more reliable age control for dating the C/T boundary. In order quantitatively to explain the carbon isotope curve and the measured TOC mass accumulation rate, a simple dynamic model of the isotope effects of organic versus inorganic carbon burial was developed. In order to verify the consistency of the model we correlated the modeled output of the Furlo section with that of the Manilva section, in southeast Spain. The modeling shows that increasing productivity only partially explains the measured $\delta^{13}C$ excursion and is not the only factor relevant to black shales deposition. Preservation may play a central role, especially in the later stages of OAE 2. Phosphorus and TOC accumulation patterns in the Bonarelli Level in both Furlo and Manilva suggest a similar process although other factors may also be involved.

Keywords: Cenomanian/Turonian; Stable isotopes; Organic matter; Modelling; Furlo; Italy; Manilva; Spain

1. Introduction

During the Cretaceous, the deposition of organic-rich black shales (with >5% total organic carbon (TOC) was common throughout the world in various palaeogeographic settings. These black shales reflect episodes of anomalous environmental conditions, which have been called ''oceanic anoxic events'' (OAEs). Two major OAEs are recorded in the Cretaceous: during the Aptian/Albian transition (OAE 1a–c) and OAE 2 at the C/T transition, also known as the ''Cenomanian/Turonian boundary event'' (Schlanger and Jenkyns, 1976; Ryan and Cita, 1977; Jenkyns, 1980). The Cenomanian/Turonian boundary event occurred during a peak global greenhouse interval, thought to be caused by a period of major oceanic crust production and volcanism which coincided with a eustatic sea level rise of nearly 300 m, relative to present levels (Schlanger et al., 1981; Larson, 1991; Kauffman, 1995). The biogenic carbonate fraction and organic matter from Cenomanian/Turonian boundary event marine sediments record a 2‰

* Corresponding author.
E-mail address: haydon.mort@unine.ch (H. Mort).

positive excursion in carbon stable isotope ratios (Schlanger et al., 1987; Kuhnt et al., 1988; Pratt et al., 1993; Accarie et al., 1996; Kolonic et al., 2002; Tsikos et al., 2004). Biostratigraphic studies suggest that the isotopic excursion represents a global oceanic geochemical event that can be used as a stratigraphic tool (Schlanger et al., 1987; Thurow et al., 1988).

The relative roles of productivity and preservation in the organic-rich sediments of the Cenomanian/Turonian boundary event are poorly understood. Some workers interpret this enrichment as caused by higher primary productivity, a consequently strong oxygen depletion, especially in deep waters, leading to enhanced preservation (Kuhnt et al., 1990; Pedersen and Calvert, 1990; Caron et al., 1999; Premoli-Silva et al., 1999). Intensified upwelling and increased ecological niche availability are some factors that can lead to higher productivity (Martinez et al., 1996).

Alternatively, a model involving preservation, would invokesluggish circulation and associated anoxia as the primary cause of improved preservation, which is not necessarily associated with productivity. In this model, a decreased oxygen exchange between the different water masses separated by a pycnocline, or a poor chemical and/thermal stratification (e.g., the stagnant basin of the Black Sea) is the primary cause (Shimkus and Trimonis, 1974; Demaison and Moore, 1980; Bralower and Thierstein, 1984).

In the Umbria-Marche Apennines, the Cenomanian/Turonian boundary event resulted in the deposition of an organic-rich interval which consists of black mudstone and shale alternating with black-grey radiolarian-rich mudstone (chert). This is called the Bonarelli Level (BL) and represents a regional stratigraphical marker. Its age is close to the Cenomanian/Turonian boundary and it varies in thickness between 1 and 2 m. The Bonarelli Level occurs in the uppermost part of the Scaglia Bianca Formation, which consists of pelagic limestones of mainly Cenomanian age (Bortolotti et al., 1970; Jenkyns, 1980; Arthur and Premoli-Silva, 1982; Coccioni et al., 1991). A correlation with the principle geochemical proxies was made with the Cenomanian/Turonian boundary in the Manilva section, southeast Spain, whose regional expressions in the Betic Cordillera have been studied by Kuhnt et al. (1990) and by Reicherter et al. (1994). The lithology and proposed palaeobathymetry of Manilva are similar to those of Furlo. By directly comparing the two sections firmer conclusions can be made.

The aim of this study is to evaluate the mechanisms of organic matter accumulation and preservation during the Cenomanian/Turonian transition. For this purpose, planktonic foraminiferid biostratigraphy, organic matter, bulk rock carbon isotope and phosphorus analyses were conducted on samples from the Furlo section, in the northern Apennines, Italy. Based on these data, a quantitative model of isotopic and organic matter interactions in a surface water ocean was developed. The comparison between our analyzed and calculated data provides some insights into the relative roles of productivity and preservation during the Cenomanian/Turonian boundary event. In addition, we present results ran on the same model for the Manilva section in order to get a better understanding of the significance of our model output. Correlating the model with TOC and P data from both sections has enabled a greater understanding of the geochemical processes involved in the generation of the modeled outputs.

2. Methods

The Furlo Section was sampled at a high resolution (10 cm intervals) with a total of 111 samples collected from the Scaglia Bianca Formation, including the Bonarelli Level. Thin sections were made for all samples for microfacies observations and micropalaeontological analysis. The limestones do not allow examination of planktonic foraminiferids in washed residues and hence biostratigraphic analysis merely examines the presence or absence of different species found in thin sections.

For stable isotope analysis samples from the Bonarelli Level were first decarbonated and then analyzed at the stable isotope laboratory of the Department of Mineralogy and Geochemistry at the University of Karlsruhe, Germany, using an Optima (Micromass, UK) gas mass spectrometer. This was equipped with an online organic matter preparation line (Carlo Erba, CSN 1030) and with an online carbonate preparation line (MultiCarb) for other samples. Separate capsules were used for each sample. The results were calibrated to PDB scale with standard errors of $<0.06‰$ for $\delta^{13}C$.

The origin and amount of organic matter were determined by Rock-Eval pyrolysis using a Rock-Eval 6 at the Geological Institute of the University of Neuchâtel, Switzerland. Errors were $<0.1\%$. Standard notations are used: TOC content in weight %; hydrogen index ($HI = S_2/TOC \times 100$) in mg hydrocarbons per g of TOC; oxygen index ($OI = S_3/TOC \times 100$) in mg CO_2 per g of TOC.

Bulk rock XRD analysis was also conducted at the Geological Institute of the University of Neuchâtel, Switzerland, using a SCINTAG XRD 2000 Diffractometer following the procedure outlined by Kübler (1987) and Adatte et al. (1996). Errors were $<5\%$. Bulk rock contents were obtained using standard semiquantitative techniques based on external standardization. Analysis of total phosphorus was conducted with a UV/Vis Perkin Elmer Lambda 10 spectrophotometer at the University of Neuchâtel, using the ascorbic acid molybdate blue developed by Eaton et al. (1995). Errors were $<5\%$.

3. Lithology

The Furlo section is located on the southwestern flank of the Furlo anticline, between the summit of the Monte Pietralata and the village of Furlo, where the Via Flaminia crosses the Bottaccione Gorge (Fig. 1A). The strata dip 40° southwest without any visible major tectonic disturbance. Samples were taken from a 12.70 m thick sequence at 10 cm intervals (Fig. 1B).

The Furlo section is part of the Scaglia Bianca Formation, which consists mainly of white limestone and mudstones (Fig. 2). At the base of the section, chert beds, varying from $1-2$ cm to 5 cm thick, are common alternating with white

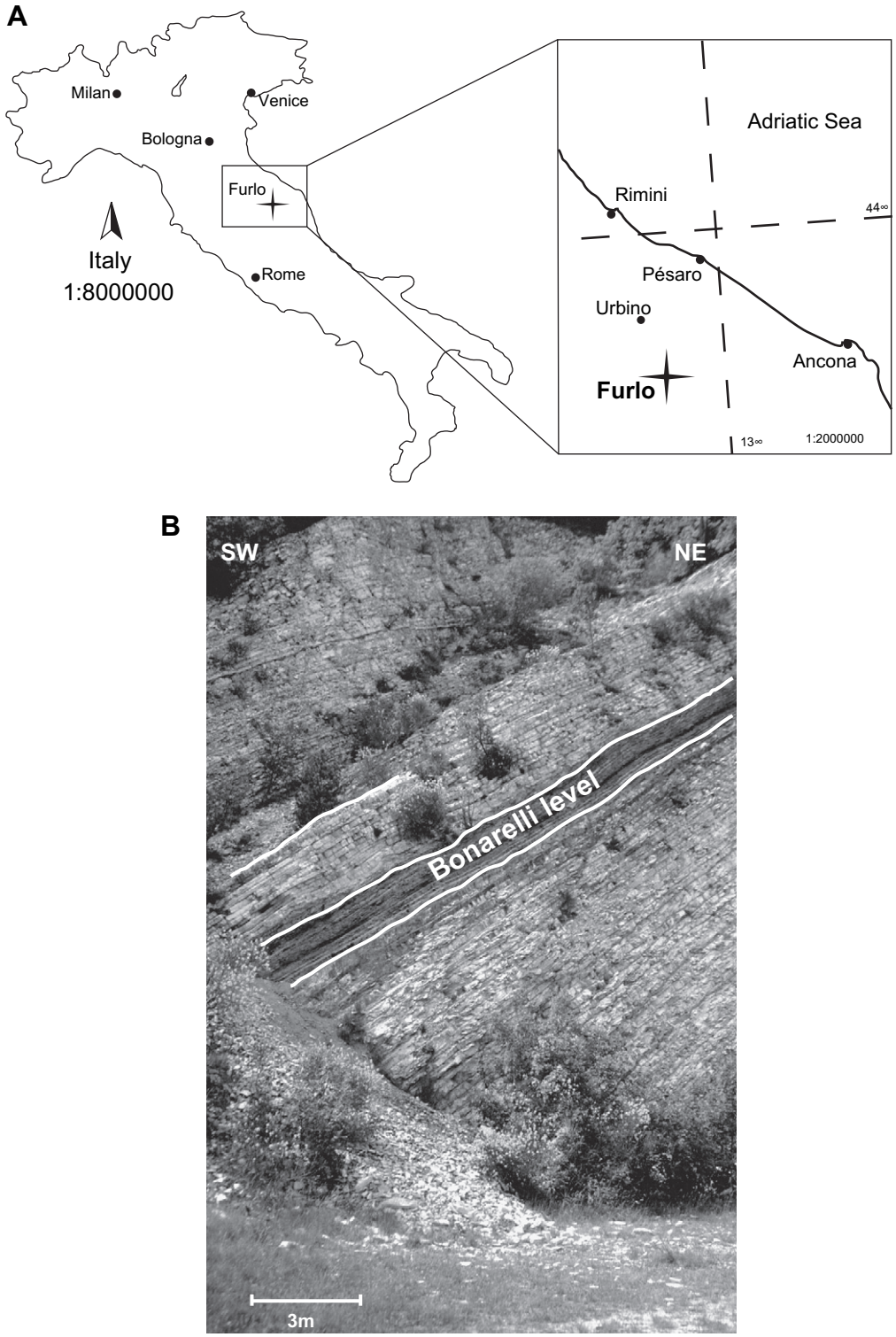

Fig. 1. (A) Geographical location of the Furlo Section, Italy. (B) General view of the Furlo Section. The Bonarelli Level and the top of the sampled section are highlighted.

limestone beds that range from 10 cm to 70 cm. The cherts consist of radiolarian-rich beds generally of a grey-black colour which are finely laminated. The upper part of the Scaglia Bianca Formation, the black Bonarelli Level (Bortolotti et al., 1970; Cresta et al., 1989) is 1.5 m thick and contains mainly finely laminated organic-rich shales and radiolarian sands. Above the Bonarelli Level, the lithology consists of rhythmically bedded 10−20 cm-thick non-bioturbated white limestones, which occasionally contain chert nodules or 1−8 cm-thick chert beds (Fig. 2A, B). Microfacies analysis shows

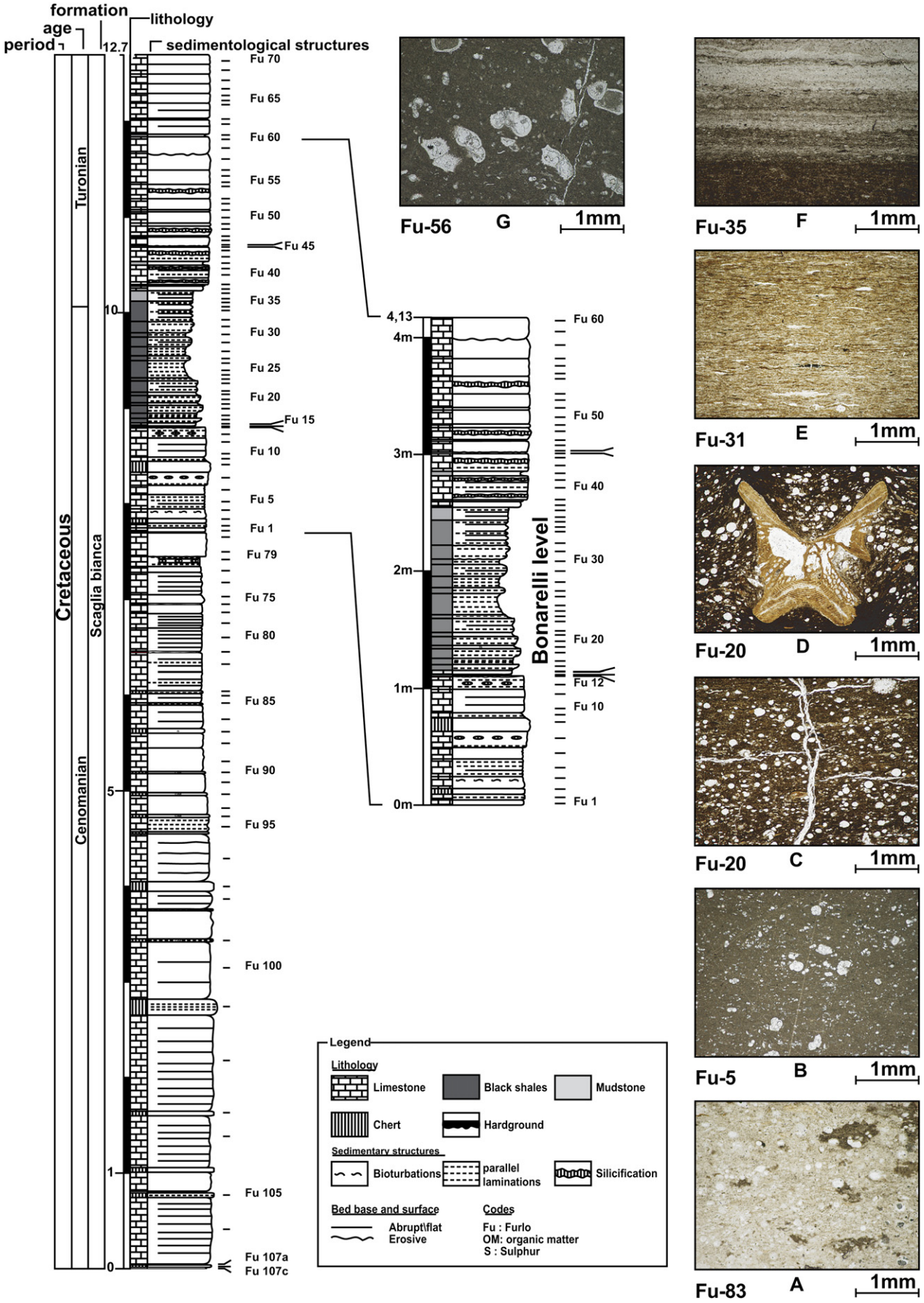
formation
age
period
lithology
sedimentological structures
Cretaceous
Cenomanian
Turonian
Scaglia bianca
12,7
10
5
1
0
Fu 70
Fu 65
Fu 60
Fu 55
Fu 50
Fu 45
Fu 40
Fu 35
Fu 30
Fu 25
Fu 20
Fu 15
Fu 10
Fu 5
Fu 1
Fu 79
Fu 75
Fu 80
Fu 85
Fu 90
Fu 95
Fu 100
Fu 105
Fu 107a
Fu 107c
4,13
4m
3m
2m
1m
0m
Bonarelli level
Fu 60
Fu 50
Fu 40
Fu 30
Fu 20
Fu 12
Fu 10
Fu 1
Fu-56 G 1mm
Fu-35 F 1mm
Fu-31 E 1mm
Fu-20 D 1mm
Fu-20 C 1mm
Fu-5 B 1mm
Fu-83 A 1mm
Legend
Lithology
Limestone
Black shales
Mudstone
Chert
Hardground
Sedimentary structures
Bioturbations
parallel laminations
Silicification
Bed base and surface
Abrupt\flat
Erosive
Codes
Fu : Furlo
OM: organic matter
S : Sulphur

high faunal diversity, with common large planktonic foraminiferids in the white limestones, and abundant siliceous organisms, such as radiolarians, silicoflagellates or diatoms, in the chert beds.

Just below the last chert bed (Fu-8) beneath the Bonarelli Level, foraminiferids rapidly decrease in abundance (Fu-6 and Fu-5) and become almost totally absent in sample Fu-7. This was also observed for chert-limestone beds above and below the Bonarelli Level. At the base of the Bonarelli Level and up to sample Fu-23, within the Bonarelli Level, radiolarians are abundant and diverse, occurring with large amounts of biogenic fragments consisting of vertebrate (fish) remains, surrounded by laminated organic matter. In the upper part of the Bonarelli Level, phosphatic fish fragments are still present, though radiolarians and silicoflagellates (not shown) are less common. Above this interval, the sediments change from black to orange-brown in colour, indicating that phosphorus is still present but perhaps not bound to organic matter. Both the black and orange-brown sediments consist mainly of organic matter and quartz/opal CT due to the presence of siliceous organisms and near-absence of large foraminiferids (Figs. 2, 3).

4. Biostratigraphy

The biostratigraphy of the Furlo section is based on planktonic foraminiferids. These are abundant and provide an additional tool for global correlation. Due to the palaeogeographic setting (deep sea basin), no ammonites were found. Relative abundances of planktonic foraminiferids, radiolaria, silicoflagellates and diatoms were estimated from thin sections. A total of 19 planktonic species were identified; smaller species of the genera *Hedbergella*, *Globigerinelloides* or *Heterohelix* were not identified to species level (Fig. 3). The base of the section (samples Fu-107c to Fu-98) is part of the upper *Rotalipora reicheli* Zone. The *Rotalipora cushmani* Zone is recognized above this interval (Fu-98 to Fu-8). The *Helvetoglobotruncana helvetica* Zone, the base of which marks the Cenomanian/Turonian boundary, appears in the top metre of the section (Fu-64) along with a species belonging to the genus *Marginotruncana*. Between the *Rotalipora cushmani* and *Helvetoglobotruncana helvetica* zones, the *Whiteinella archeocretacea* Zone (Fu-8 to Fu-64) is tentatively identified. This interval corresponds primarily to the Bonarelli Level and planktonic foraminiferids are mostly absent up to sample Fu-48 (Fig. 3). In the upper part of the *W. archeocretacea* zone, larger species are present, including *Dicarinella hagni*, *Marginotruncana sigali*, *Praeglobotruncana gibba* and *P. stephani*.

The larger and more complex ornate foraminiferid species (K-species) are generally more sensitive to changing environmental conditions. This is due largely to their highly specialized niche selection, generally subsurface habitat, and preference for oligotrophic conditions. In the Furlo section, the K-species taxa (belonging to the genera *Rotalipora*, *Dicarinella* and *Praeglobotruncana*) are present above and below the Bonarelli Level where environmental conditions were favourable. The smaller species, belonging to the genera *Whiteinella*, *Hedbergella*, *Globigerinelloides* and *Heterohelix* were more tolerant of environmental changes (R-species), including changes in oxygen, salinity and nutrients. R-species taxa generally reproduce rapidly, are very abundant, inhabit surface and subsurface waters and hence are considered opportunists (McArthur and Wilson, 1967; Caron, 1983). These species are generally common in the organic-rich shales of the late Cenomanian $\delta^{13}C$ excursion (Leckie, 1985, 1987; Keller et al., 2001). In the Furlo section, however, these stress tolerant species are nearly absent in the Bonarelli Level, possibly due to dissolution.

5. Stable carbon isotopes and age control

The observed $\delta^{13}C$ trends are very similar to published curves based on bulk rock, fine fraction carbonates, planktonic foraminiferids and organic matter across OAE 2 (Scholle and Arthur, 1980; Accarie et al., 1996; Nederbragt and Fiorentino, 1999; Paul et al., 1999; Keller et al., 2001; Keller and Pardo, 2004). The major features of the organic matter $\delta^{13}C$ OAE 2 excursion at Furlo are: (1) a rapid increase of 3‰ towards a first peak; (2) a 0.7‰ decrease forming a trough; (3) a 1‰ increase to form the second peak; and (4) prolonged high $\delta^{13}C$ values into the early Turonian (Fig. 4). The same features have been identified at the Pueblo GSSP (Pratt, 1985; Keller et al., 2004) and at Eastbourne, England (Gale et al., 1993; Paul et al., 1999; Keller et al., 2001), suggesting that this pattern reflects a series of widespread or global oceanographic events (Fig. 4). Whilst it is true that carbon isotope values derived from organic matter are subject to the origin of the organic matter, we are confident that the signal is productivity-derived due to the similarities with the signatures from Pueblo and Eastbourne. In the absence of carbonate it provides the best proxy we have for measuring productivity. Carbonate carbon isotope values below and above the Bonarelli Level are stable without considerable variation. This also indicates that the excursion seen in Furlo has longer term significance. The nature of the $\delta^{13}C$ excursion is, however, different from those in these shallower sections and more similar to deeper more pelagic sediments such as those found close by in the Gubbio Section (Tsikos et al., 2004). In these types of sections, where $\delta^{13}C$ is invariably measured using organic matter, the isotope plateau tapers off extremely rapidly. Tsikos et al.

Fig. 2. General and detailed log of the Furlo Section and Bonarelli Level with associated main microfacies. The grey scale of the sedimentary column was chosen according to the field observations. Thin section Fu-83 (A): typical chert bed with radiolarians and organic matter, Fu-5 (B): wackestone with high diversity of foraminiferids (*Rotalipora*, *Hedbergella*) below the Bonarelli Level, Fu-20 (C and D): black shale with radiolarians and biogenic phosphate fragments, respectively with a fish vertebrate, Fu-31 (E): laminated black shale with phosphate microfilms, Fu- 35 (F): black shale/mudstone, indicating carbonate production, Fu-56 (G): Wackestone with foraminiferid assemblages (*Dicarinella*, *Whiteinella*).

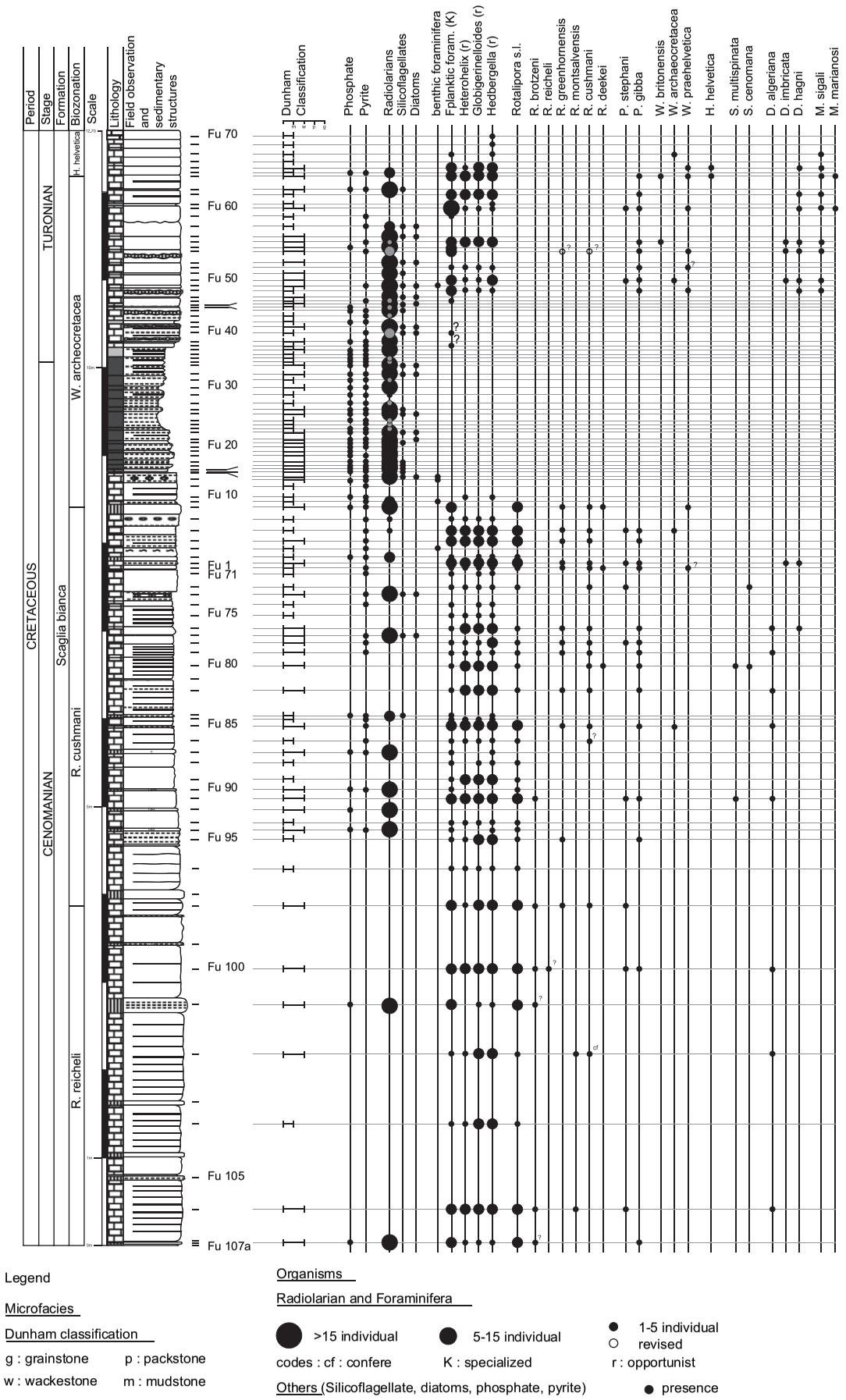

Fig. 3. Foraminiferid distribution and biostratigraphy across the Cenomanian–Turonian boundary at Furlo.

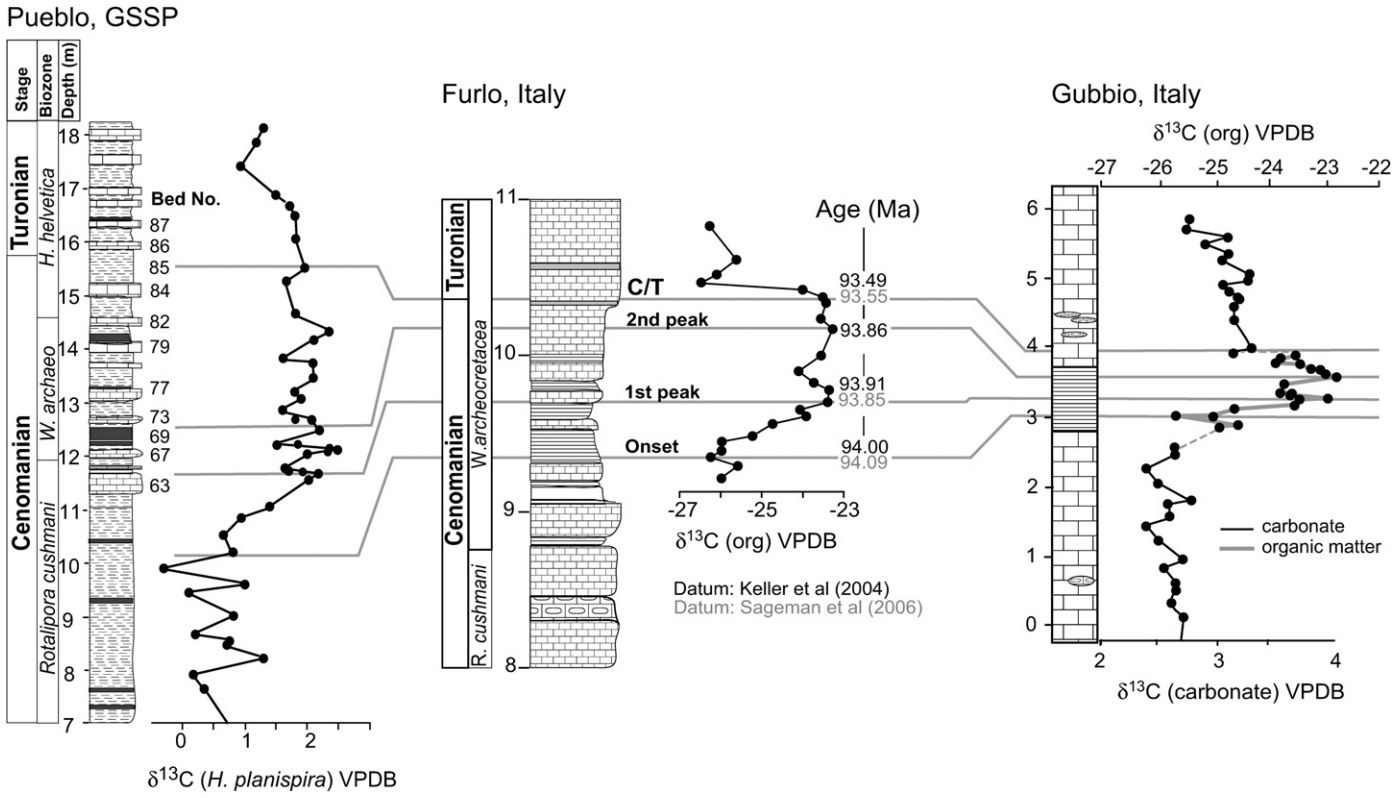

Fig. 4. Variations in $\delta^{13}C$ isotopic composition through the Bonarelli Level at Furlo and Gubbio (Tsikos et al., 2004), correlated with the Pueblo Section GSSP. Also plotted are the ages assigned to the various points on the Furlo $\delta^{13}C$ curve extrapolated from Keller et al. (2004) and Sageman et al. (2006).

(2004) explained this through changes in regional productivity or hiatuses, although this has not been tested. However this rapid tapering does not concern this study, which focuses on the basal part of the section, of which the isotope stratigraphy appears intact.

In both sections planktonic foraminiferid datum events and the structure of the $\delta^{13}C$ excursion are comparable. Age estimates for species first and last appearances, $\delta^{13}C$ excursions and depositional and environmental events have been calculated by Keller and Pardo (2004). These are based on ages of various ammonite and planktonic foraminiferid datum events extrapolated from the radiometric dates (Hardenbol et al., 1998) and are compatible (Keller et al., 2004) with three $^{40}Ar/^{39}Ar$ ages determined from bentonite layers (Obradovitch, 1993; Kowallis et al., 1995; Snow et al., 2005).

The Furlo section is calibrated with the Pueblo section using ages given by planktonic foraminiferid biostratigraphy and $^{40}Ar/^{39}Ar$ dating from bentonites (Hardenbol et al., 1998; Keller et al., 2001; Keller and Pardo, 2004). Assigned ages are as follows: the isotopic onset (94.00 ± 0.2 Ma), the two-peaked $\delta^{13}C$ shifts (93.91 ± 0.2 and 93.89 ± 0.05 Ma respectively), and the Cenomanian/Turonian boundary level corresponding to the first appearance of the ammonite *Watinoceras devonense* (93.49 ± 0.2 Ma) or, in our case, to the prolonged high $\delta^{13}C$ values (Fig. 4). The onset of the rapid $\delta^{13}C$ excursion at Furlo begins at the base of the Bonarelli Level (Fu-19), and reaches a maximum at Fu-25 (see Fig. 6 for sample distribution). The isotopic values then decrease rapidly from Fu-34 corresponding to the last black shale, or to the Cenomanian/Turonian boundary, which is estimated at Furlo based on a correlation with the Pueblo section.

In the Furlo section, the last appearance of *R. cushmani* in sample Fu-8 significantly predates the first $\delta^{13}C$ shift, the extinction datum of this species in other sections (e.g., Tunisia, Italy, Spain, France, England, USA; Lamolda et al., 1994; Nederbragt and Fiorentino, 1999; Paul et al., 1999; Keller and Pardo, 2004). This is probably an environmental effect at Furlo associated with the removal of carbonate at the Bonarelli Level. Similarly, *Helvetoglobotruncana helvetica* appears later at Furlo, due either to environmental changes, difficulties in determining the evolutionary transition from *Praeglobotruncana praehelvetica* to *H. helvetica*, or to diachronous evolutionary transition of these species. For these reasons, the correlation with the Pueblo section is based largely on a combination of biostratigraphy and the $\delta^{13}C$ curve. This correlation suggests that the Furlo Section is condensed but reasonably complete, similar to the Gubbio section (Tsikos et al., 2004). The timing of the Cenomanian/Turonian boundary event can therefore be constrained by using the ages associated to the $\delta^{13}C$ peaks (Keller et al., 2001, 2004).

6. Mineralogy

Bulk rock mineralogy was determined for 60 samples encompassing the Bonarelli Level (Fig. 5). Quartz, calcite,

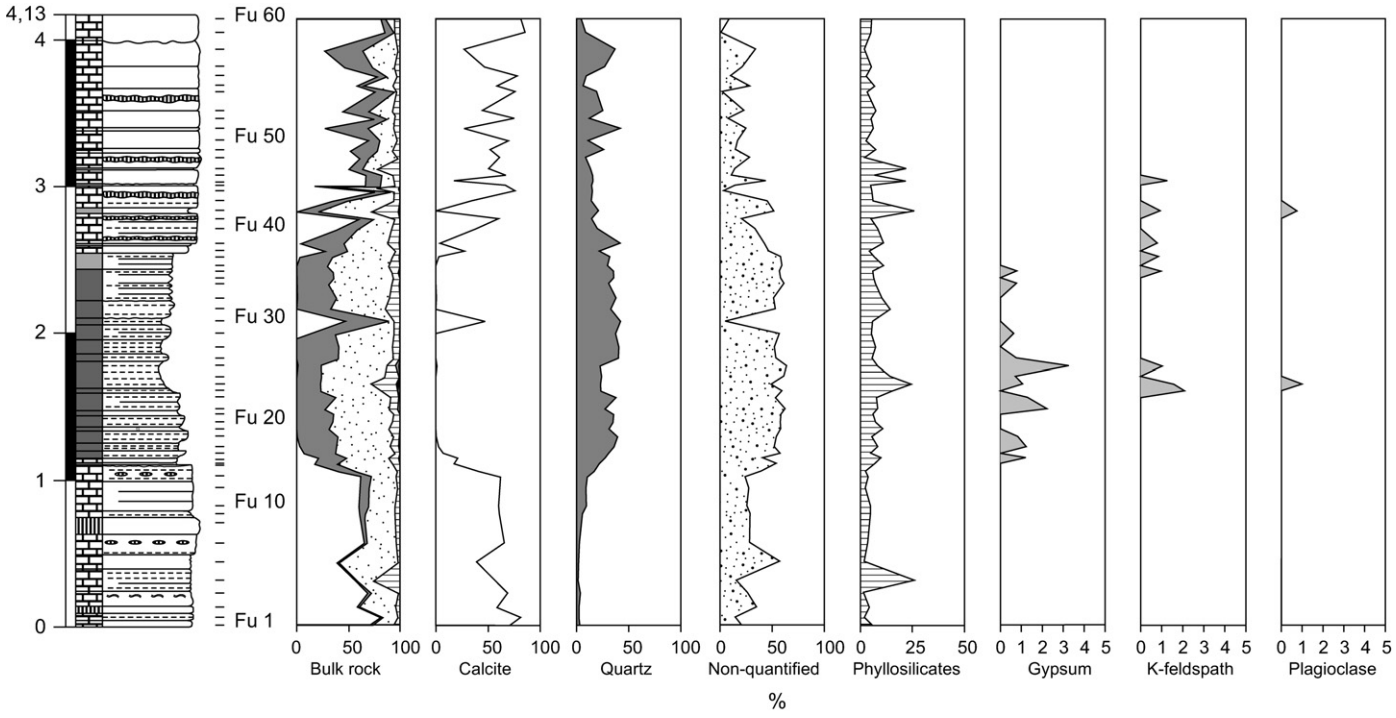

Fig. 5. Bulk mineralogy of the Bonarelli Level. Non-quantified minerals correspond mainly to organic matter and nearly amorphous biogenic quartz.

phyllosilicates, and 'non-quantified' were the four major groups observed. Minerals such as gypsum, Na-plagioclase, or K-feldspar were also identifiable in smaller quantities. Quartz abundance is low at the base of the section but increases rapidly up-section through the Bonarelli Level. Calcite abundance is inverse to quartz, with very low values in the BL. Non-quantified minerals represent the sum of minerals/phases that were not recognized by XRD analysis. However, in this study the non-quantified phases are thought to mainly correspond to organic matter and nearly amorphous to microcrystalline biogenic quartz (Fig. 5).

Based on the results obtained, the section can be subdivided into two parts: the Bonarelli Level and the white limestones. The Bonarelli Level is essentially composed of organic matter and quartz/opal CT. The presence of radiolaria explains the high quartz/opal CT content. Planktonic foraminiferids are rare in the Bonarelli Level. The large amount of organic matter present in the bottom waters results in acidification and dissolution, which may explain the near-absence of foraminiferids in the Bonarelli Level. After carbonate removal, rare silicified ghosts of foraminiferids have been recognized in the insoluble residue. Before and after the Bonarelli Level, white limestones with lower quartz content and diverse foraminiferid assemblages indicate an oligotrophic pelagic environment.

7. Organic matter

The Bonarelli Level is nearly devoid of carbonate (<7.05%), except for the basal and uppermost parts, which contain up to 21% and 28% respectively (Fig. 5). The TOC record reflects the quantity of organic matter, although it should be kept in mind that organically bound oxygen, hydrogen, sulphur and nitrogen can contribute up to 50% of the total sedimentary organic matter (Tissot and Welte, 1984). The TOC content is highly variable, ranging from 0.66% to 17.09% (Fig. 6). The TOC content increases gradually in the Bonarelli Level to a first maximum at Fu-22 (9.25% TOC). After some fluctuations, the second maximum is reached at Fu-26 (13.58% TOC), with the maximum value recorded in sample Fu-31 (17.09% TOC).

Information on the composition and maturity of organic carbon can be achieved by pyrolysis measurements (Espitalié et al., 1985; Crumiere et al., 1990). With this method, the type of organic matter is determined by the hydrogen index (HI) and the oxygen index (OI), which approximate to the H/C atomic ratio and O/C atomic ratio respectively. Based on the observed range of HI-values (268−564 mg HC/g TOC) and of OI-values (23−57 mg CO_2/g TOC), the organic matter of the BL is distributed in the field of type 2 organic matter (Fig. 7), which is associated with marine environments (Espitalié et al., 1985). The high HI values also suggest well-preserved organic matter. Temperatures of maximum pyrolytic hydrocarbon yield (T_{max}) are in the range of 402−433 °C for samples having an organic-richness higher than 0.75% TOC. This indicates that the organic matter did not experience strong burial and is still immature with respect to oil-generation.

8. Sedimentation and mass accumulation rate

Ages obtained by biostratigraphic and carbon stable isotope correlation with the Pueblo section allow calculation of the

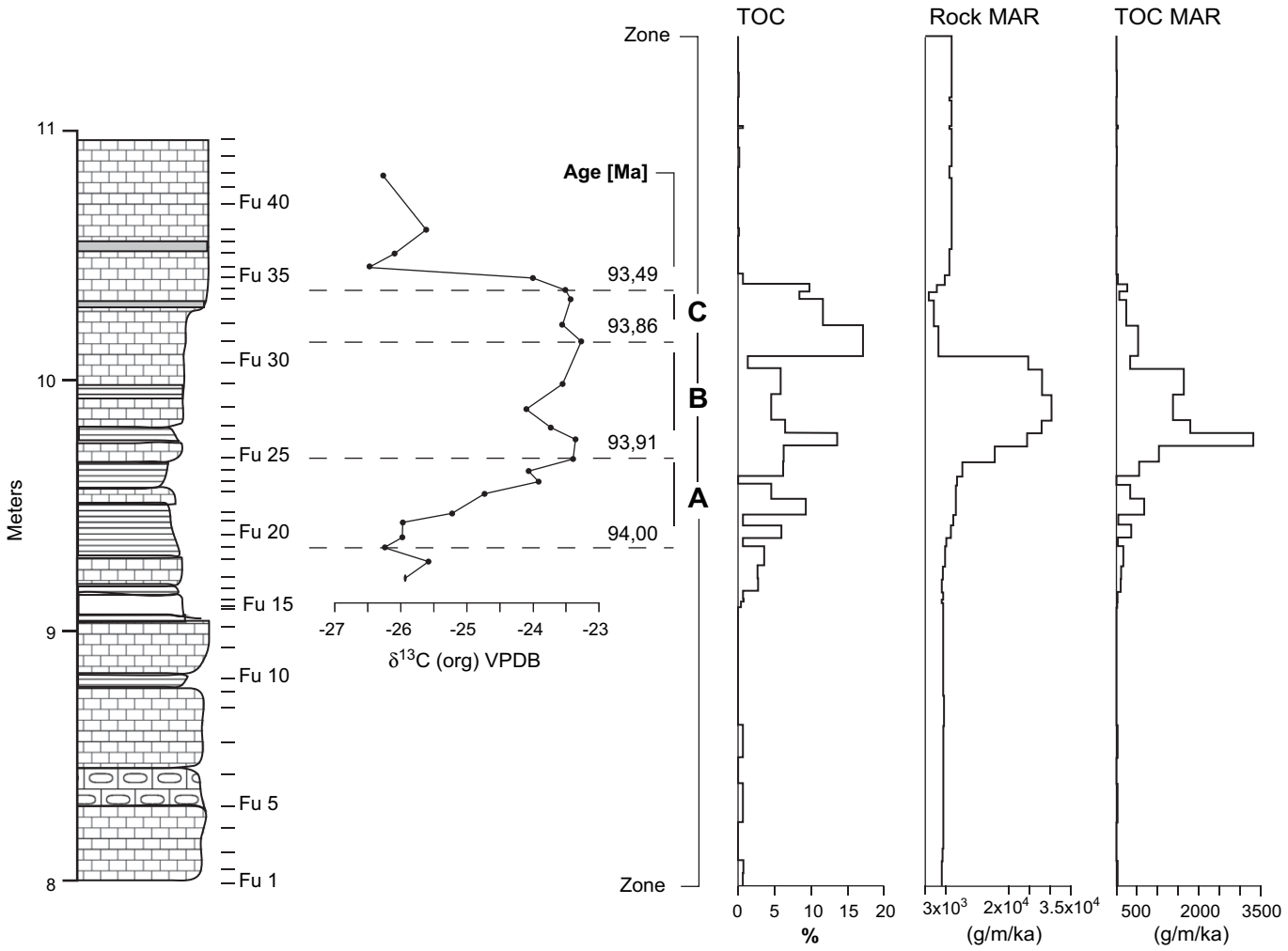

Fig. 6. $\delta^{13}C$ isotopic composition and related correlated age, with TOC values and respective rock and TOC mean accumulation rate.

average sedimentation and mass accumulation rates for the different intervals. Each interval for which an age was determined was separated into two parts to improve the resolution. The first dated interval (identified as 'A'; Fu-19 to Fu-25) was calculated to have a non-decompacted sedimentation rate of 0.38 cm/ky. Interval B (Fu-25 to Fu-31), sees the sedimentation rate more than double to 0.88 cm/ky. In interval C (Fu-31 to Fu-34), the sedimentation rate drops to a minimum value of 0.055 cm/ky. The average sedimentation rate calculated for the whole interval (A—C) is 0.19 cm/ky.

To better estimate the contribution of the various lithologies, the mass accumulation rate in $g/m^2/ky$ was calculated for each interval from A to C (Fig. 6). The rock densities for black shales, marls, cherts and limestones were taken from Attewell and Farmer (1976). To avoid a different mass accumulation rate for the same sample, the following corrections were applied. The mass accumulation rate for dated horizons (Fu-19, Fu-25, Fu-31, and Fu-34) taken as the average of the upper and lower mass accumulation rates. The curve was then smoothed to constrain the proposed mass accumulation rate for each zone. Although inherently imperfect, the resulting curve corresponds better to the probable environmental conditions. The last age of 93.49 Ma (Fu-34), with an error margin of 0.2 Ma, generates an error because the lower error limit of 93.29 Ma is chosen, in which case the mass accumulation rate doubles. The mass accumulation rate curves for both rock and TOC represent maximum values, assuming that the calculated ages are reliable. However, this correction does not change the general shape of the curve, because the thickness for interval 'C' remains small. The other intervals are more precise (error margins of 0.2 or 0.05 Ma), and therefore no correction factor was applied.

The mass accumulation rate of TOC was calculated in the same way (Fig. 6), multiplying TOC values with rock mass accumulation rates. Both values of rock and TOC mass accumulation rates increase gradually from the basal part of the Bonarelli Level, then decrease rapidly in the uppermost layers, around Fu-31. The lower sedimentation rate, for interval 'C', may be due to decreased biogenic productivity and/or non-deposition. However, as previously mentioned, based on correlations with the Pueblo section, the Furlo section though condensed, still seems relatively complete. The average rate of 0.19 cm/ky compares well with the average rates of 0.5—1.0 cm/ky (Elder and Kirkland, 1985), 0.9 cm/ky

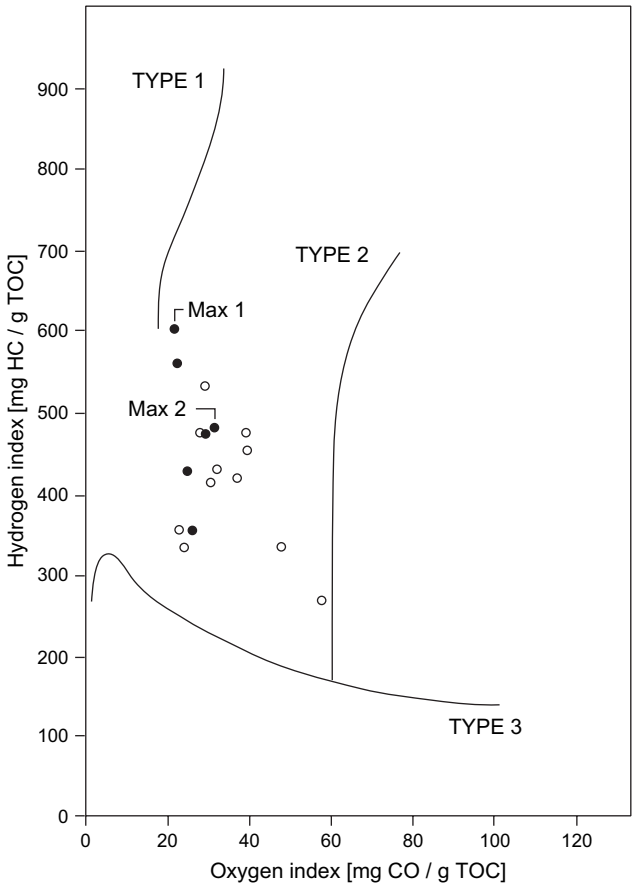

Fig. 7. Espitalié diagram. All data are within the type 2 field, indicating organic matter of marine origin. Maximum 1 indicates Fu- 31, and Maximum 2 Fu-26. Black points refer to values greater than 8% TOC.

(Scott et al., 1998) and 0.57 cm/ky (Sageman et al., 1998) for the shallower environment of the Pueblo section. The major sedimentary break or discontinuity between the B and C intervals may be a biostratigraphic artifact (e.g. delayed or variable first appearance of *H. helvetica* (93.49 or 93.29 Ma given by (Hardenbol et al., 1998), ±0.05 Ma). A more precise age can be calculated based on the carbon isotope shifts (error margin of 0.2 Ma; Keller et al., 2004). The average sedimentation rates of the basal part of the Bonarelli Level (interval A: 0.38 cm/ky and B: 0.88 cm/ky), which are calculated using well-dated carbon isotope shifts, show a significantly lower sedimentation rate than the figure of 10 cm/ky proposed by Beaudoin et al. (1996).

9. Phosphorus mass accumulation rate

All of the samples from Furlo and Manilva were analyzed for total phosphorus content. In this paper, only the data from the Bonarelli Level are presented (Fig. 8). The concentration of phosphorus (mg/g) and mass accumulation rate is calculated (mg/cm^2/kyr). A recent study by Sageman et al. (2006) constructed a high-resolution cyclostratigraphy timescale based on harmonic analysis developed by Meyers et al. (2001) and Meyers and Sageman (2004). The ages derived from this study were used to construct separate P mass accumulation rates, which allowed us to better assess how sedimentation rates effects our phosphorus results.

Like organic matter, phosphorus (P) increases rapidly in the Bonarelli Level. With the appearance of black shales, the first peak is observed between Fu-19−23 (0.027 [mg/g] and 0.017 [mg/g] respectively, Fig. 8). Above this interval, values decrease rapidly and reach a second peak at Fu-29 (0.02 [mg/g]). In the uppermost part of the Bonarelli Level as well as in the white limestones, P is very low (0.005 [mg/g]). Precisely the same trend is observed in the Manilva section, although values of TOC and P mass accumulation rates are considerably higher.

Sinks for phosphorus include organic matter, skeletal matter, iron and manganese oxyhydroxides, clays and phosphate minerals, incorporated into and preserved in sedimentary reservoirs (Föllmi, 1996). The increase in TOC and P mass accumulation rates is concordant at Furlo and Manilva (possible slightly before in Manilva) but the origins of P are likely to be different. In the basal part of the black shales, rock and TOC mass accumulation rates are low, contrary to those of phosphorus. P, therefore, does not appear to be bound principally to organic matter, even though there is an abundance of it. Biogenic phosphate fragments (fish vertebrates, fish bones), and biogenic fragments rimmed by phosphate, are common and associated with abundant radiolarians (bed 20, Fig. 2). Authigenic phosphorus is therefore likely to be the dominant phosphorus reservoir in the Furlo section.

P mass accumulation rates calculated from the ages (see Fig. 4) given by Sageman et al. (2006) also generate the same general increase in P mass accumulation rate prior to the $\delta^{13}C$ peak, albeit slight earlier, at 9 m (Fu-14). The use of Sageman et al. (2006) creates a more consistent sedimentation rate. Assigning dates obtained by a high-resolution cyclostratigraphic framework onto a low-resolution $\delta^{13}C_{(org)}$ curve is difficult. Nevertheless, the results from this simple exercise support the assertion that variations in P mass accumulation rate are *not* merely an artifact of changing sedimentation rate.

10. Modelling

The positive carbon stable isotope excursion during OAEs may be explained by depletion of the inorganic dissolved CO_2 pool in ^{12}C due to increased burial of organic matter. In order to test whether this hypothesis holds quantitatively in the Furlo section, a simple stock and flux model (called ISOAE) was developed and calculated using the modeling Stella Research© (High Performance Systems Inc.). The carbon isotope profile of the Manilva section in Spain was also used to generate a modeled output. The results may be comparable as both sections probably have similar depositional environments and palaeodepths.

The ISOAE model (Fig. 9) is based on two stocks or reservoirs in the upper layers of the ocean waters: the dissolved inorganic carbon reservoir (DIC) and the reservoir of carbon bound to dissolved or suspended organic matter (OM). Four fluxes are

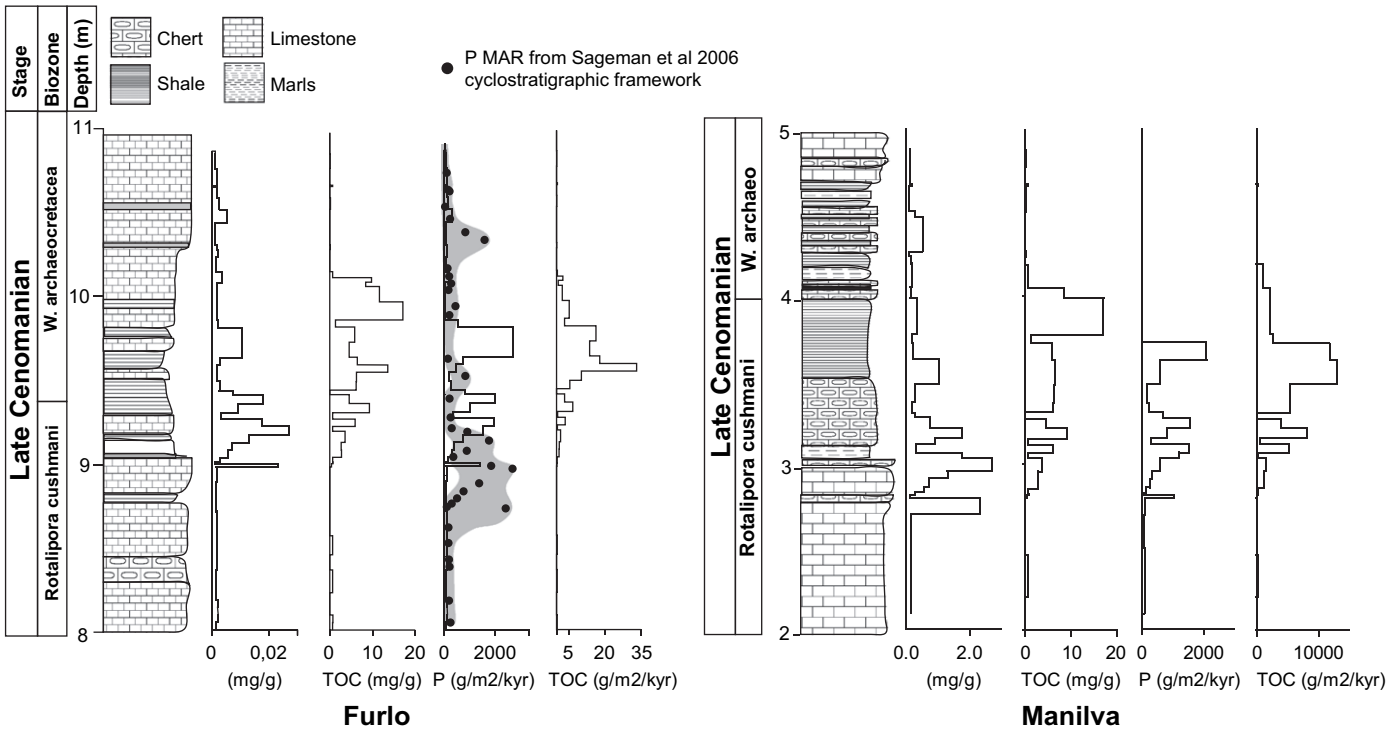

Fig. 8. Phosphorus and TOC contents (mg/g), phosphorus and TOC mass accumulation rates (g/m^2/ka) values for the Bonarelli Level in the Furlo and Manilva sections.

connected to the reservoirs: (1) the supply of inorganic carbon (CO_2) into the DIC-reservoir (Fsupply, combining volcanic release and river input), (2) the formation of OM from CO_2 i.e. photosynthesis (F_DIC_OC), (3) the burial of carbonates (F_sed_IC) and (4) the burial of organic matter (F_sed_OC).

The carbonate burial rate is set to be proportional to the size of the DIC reservoir:

$$\text{F\_sed\_IC} = f\text{Cc} * \text{DIC}$$

where fCc is the fraction of carbonate buried per unit of time. The (small) part of the DIC that enters the OC reservoir is proportional to the size of DIC and to a productivity factor $f$prod:

$$\text{F\_DIC\_OC} = \text{DIC} * f\text{prod}.$$

Finally, the burial of organic matter is set to be proportional to the OM reservoir:

$$\text{F\_sed\_OC} = \text{OC} * f\text{OM}.$$

The model is designed in such a way that each carbon isotope (^{12}C and ^{13}C) has it own reservoirs and fluxes. Thus it is possible to know at any time the isotopic ratio of each reservoir and flux. The isotopic fractionation during organic matter formation, i.e. the kinetics uptake of ^{12}C during photosynthesis, is included by a kinetic factor k12. As a consequence the equation for the flux from the DIC-pool to the OC-pool becomes:

$$\text{F\_DIC\_OC\_12} = \text{DIC\_12} * f\text{prod} * \text{k12}.$$

Before simulation can be done, all parameters must be adjusted to run the system in steady state. For this, the size of the reservoirs and input fluxes are adopted from Siegenthaler and Sarmiento (1980) with 120,000 [GtC/Mioy] for Fsupply, 970 GtC for the DIC reservoir and 3 GtC for the OM reservoir. The factors fCc, $f$prod, and fOM are calculated from the following equations describing the steady-state (input = output):

$$\text{Fsupply} = f\text{Cc} * \text{DIC} + f\text{prod} * \text{DIC}$$

$$f\text{prod} * \text{DIC} = f\text{OM} * \text{OM}$$

Moreover, the ratio of organic to carbonate carbon burial is taken to be

$$f\text{OM} * \text{OM}/f\text{Cc} * \text{DIC} = 0.06.$$

The ratio of 0.06 is given by Sarmiento et al. (2002) and also corresponds to the TOC/MINC ratio of the Fu-13 sample, which can be considered as a background ratio before the onset of the OAE 2. Finally, the ^{12}C/^{13}C ratio of Fsupply is adjusted to have an isotopic response of $+1.5‰$ in the DIC reservoir and the k12 rate constant is chosen such that the ∂^{13}C value of the OC reservoir becomes $-26‰$ in the steady state. In this model, the ∂^{13}C of the DIC reservoir increases when organic carbon burial is increased. The ∂^{13}C values of the OC reservoir follow those of the DIC reservoir, with an offset given by the kinetic factor k12 (Fig. 10). The dependence between the productivity (given by $f$prod) and the isotopic curves is almost linear.

Starting with these steady state parameters, a simulation was run, where the productivity factor ($f$prod) was varied so as to reproduce schematically the ∂^{13}C values measured in the Furlo Section. The resultant rate of organic carbon burial

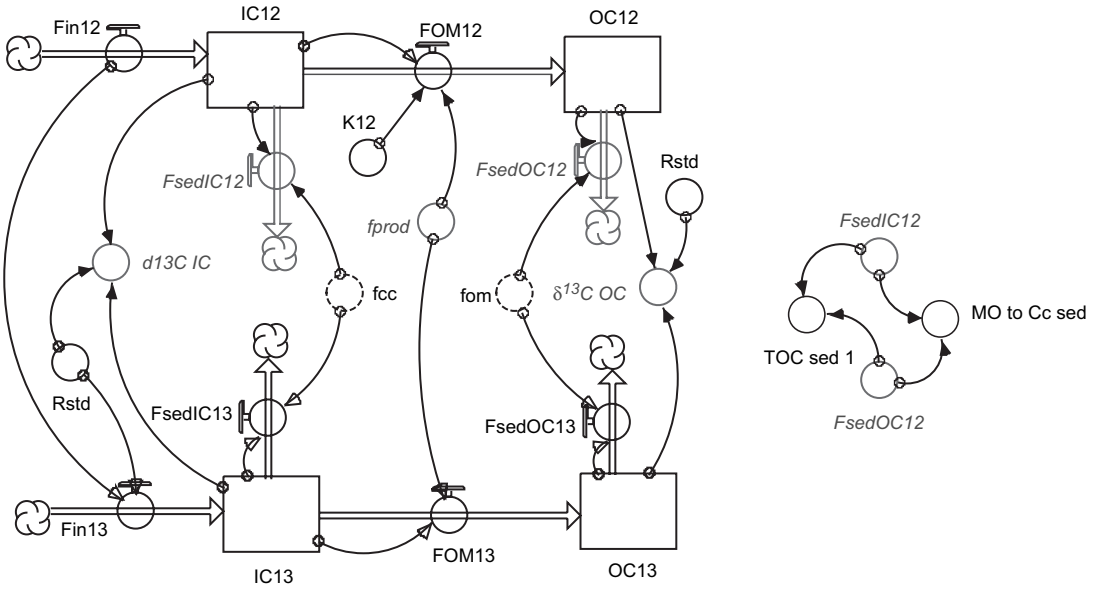

Fig. 9. The ISOAE Model design. The $\delta^{13}C$ curve for Furlo (and Manilva) is assumed to be produced by productivity alone. Using simple stock-flux mechanisms and fractionation constants, the model calculates the accumulation of organic matter. By comparing this modeled output with organic carbon values actually measured, we may make certain hypotheses as to the relative importance of productivity versus preservation. See text for details.

indeed shows a major increase in the Bonarelli Level. In Fig. 11, the normalised curves of the measured and calculated TOC accumulation rates are compared. In general, the model is able to explain the measured isotopic curve and the variations in the burial rate of organic carbon. According to the model, organic carbon burial (i.e. effect of productivity) must nearly triple (factor of 2.7) to obtain the measured isotopic excursion. Since we keep the inputs (Fsupply) constant, the ISOAE model implicitly diminishes the sedimentary flux of inorganic carbon during times of higher productivity. This may well correspond to the reality. The Cenomanian/Turonian boundary event may represent a time of global crisis in carbonate platform development (Ferrandini et al., 1985; Mermighis et al., 1991; Abdallah and Meister, 1997; Davey and Jenkyns, 1999; Buchbinder et al., 2000). With the drowning of the platforms this important sink of inorganic carbon would have been switched off (Weissert et al., 1998). In our simulation the flux of inorganic carbon is reduced by 9% at maximum burial of organic matter. As a result, the ratio of IC to OC burial changes from 16 (before and after the isotopic excursion) to 5 (during the isotopic excursion). A similar trend is observed in the Manilva section (Fig. 11). Actual OM accumulation begins to exceed modeled values at the first peak in $\delta^{13}C$.

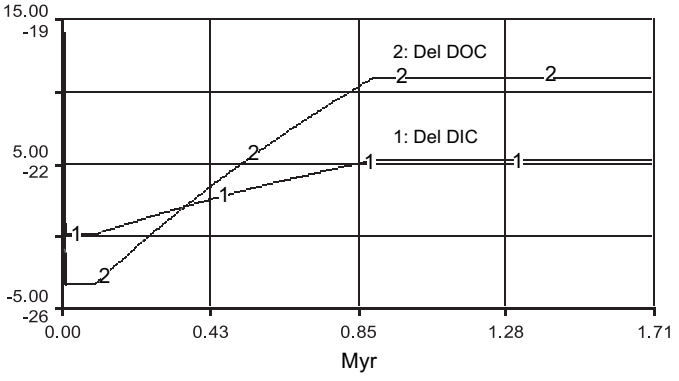

Fig. 10. Model behaviour for a 10-times increase in *f*prod over 1.7 Ma.

11. Discussion

The age of the Furlo section is well constrained, based on the shape of the $\delta^{13}C$ curve correlated with that of the Pueblo stratotype section (Keller et al., 2004). At Furlo, the major planktonic foraminiferid zones, and details of the OAE 2 $\delta^{13}C$ excursion indicate a relatively continuous but slow sediment deposition across the Cenomanian/Turonian boundary, relative to Pueblo. The upper Cenomanian succession is characterized by the Bonarelli Level, which consists of a 1.5 m thick black shale with up to 18% TOC. This level coincides with a major positive $\delta^{13}C$ excursion, which is interpreted as having resulted from a depletion of ^{12}C in the water column due to high primary productivity and/or enhanced preservation of organic matter as a result of poorly oxygenated bottom waters (Pratt, 1985).

From our simple model, it is reasonable to say that increasing the productivity factor (*f*prod) to meet the carbon isotopic constraints comfortably explains the OC burial in the basal part of the Bonarelli Level (Fu-16 to Fu-24). However, in the middle part (Fu-25 to Fu-28), the model values fall below the measured values. In other words, the ISOAE model finds it impossible that productivity alone can explain the organic carbon burial rate during this time. It is always during the $\delta^{13}C$ excursion that this discrepancy takes place in Furlo and Manilva (Fig. 11). Preservation may therefore also play a central role. This proposition is given weight when we observe the same trend in the Manilva section (Fig. 11). The very high

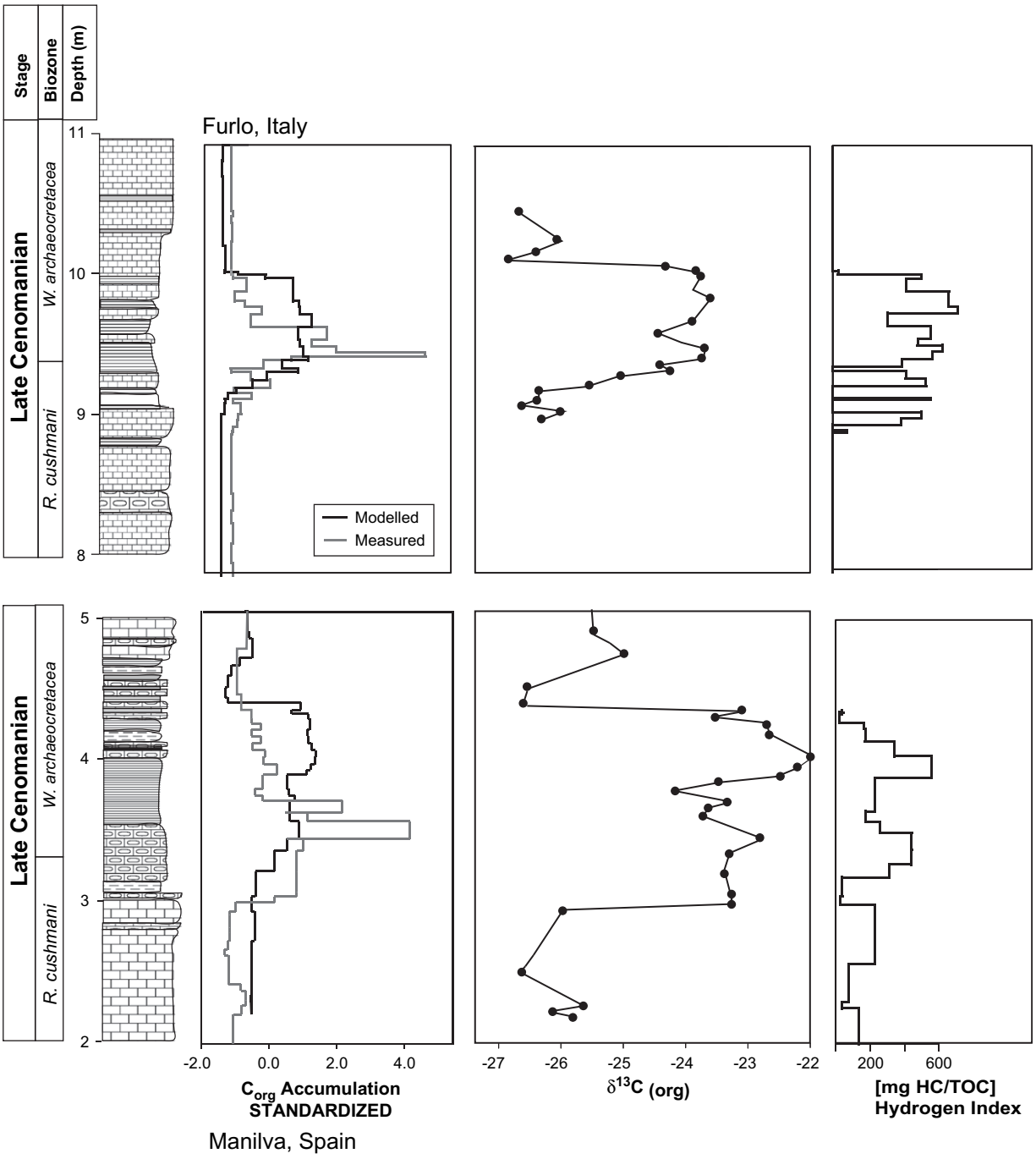

Fig. 11. From left to right: comparison of the measured and modelled OC mass accumulation rate output, $\delta^{13}C$ isotopic fluctuations and hydrogen index for the Furlo and Manilva sections.

hydrogen index values in Furlo and Manilva during the isotope excursion start and mid-plateau supports enhanced preservation over productivity.

The fact that P mass accumulation rates increase more rapidly compared to TOC mass accumulation rates in Furlo and Manilva (Fig. 8) supports the model in this respect, suggesting that increased productivity may be the main factor leading to the initial increased P, at the base of the Bonarelli Level. In contrast, in the upper Bonarelli Level, rock and TOC mass accumulation rates are high and no phosphatic biogenic fragments are observed (bed 31 and 35, Fig. 2). The sediment consists mainly of organic matter and quartz/opal CT. In bed 31, the sediment changes in colour from black to orange-brown and is finely laminated, indicating that P is still present. In this upper part, microbial activity may control the rate of P accumulation. Patterns associated with productivity processes are no longer observed. Preservation may play a more central role during this stage of the event. Large increases in the HI values during the excursion plateau (Fig. 11) are consistent with increased preservation of organic matter compared to

the lower part of the Bonarelli Level. This observation is supported by Mort et al. (2007) in which the burial efficiency of P is shown to decrease during the positive $\delta^{13}C$ excursion and plateau. P may therefore be concentrated in organic matter, which, in this case, would be preserved due to reduced oxygenation of bottom waters.

The model predicts that a 3-fold increase in productivity is required to cause the observed increased in measured $\delta^{13}C$ values. Therefore, productivity alone cannot explain the recorded increase in TOC mass accumulation rate values. Phosphorus mass accumulation rate values in the Furlo and Manilva sections are in good agreement with the modeled results, suggesting that this element is associated first with productivity and then with preservation.

All this, of course, does not help to explain what caused the increase in productivity in the first place. The apparent high productivity associated with the $\delta^{13}C$ excursion could be explained by a number of factors. For example, the complex interactions between the Cenomanian/Turonian boundary event sea level transgression, nutrient remobilization as well as CO_2 and P release from volcanic provinces may all have led to increased productivity and even eutrophic conditions in surface waters (Larson and Erba, 1999; Leckie et al., 2002). The increased accumulation of organic matter and depletion of oxygen in the water column could have led to the enhanced preservation of organic carbon, the extinction of environmentally sensitive planktonic species and the survival of low oxygen tolerant species.

Although there is good agreement between the data sets and the model, a number of additional factors should also be considered. These include: (1) Inaccurate accumulation rates due to uncertainties in the assigned ages. Indeed, the slower sedimentation rate in the upper part (0.055−0.88 cm/ky), and the subsequent lower accumulation in this upper part of the Bonarelli Level, may be due to an overestimate for the first appearance datum of the ammonite *Watinoceras devonense*, where the error margin is greater than those for the $\partial^{13}C$ shift. (2) Changes in the depositional patterns, i.e. changes in the lateral advection of OM into or out of the studied section. To improve the model a more detailed understanding of the oceanic circulation (e.g. inclusion of the deep ocean reservoir) and palaeogeography of the late Cretaceous is required. (3) Changes in magnitude (e.g. due to increased pCO_2 in the atmosphere) and isotopic composition of the input flux. (4) Changes in pCO_2 in the surface waters, due to changes in pH.

12. Conclusions

The Furlo section can be correlated with the Pueblo stratotype based on the $\delta^{13}C$ excursion. The isotope and planktonic foraminiferid biostratigraphy of the Furlo section show that it is condensed, yet relatively complete.

The Cenomanian/Turonian event is evaluated based on TOC mass accumulation rates and $\delta^{13}C$ fluctuations. To approximate the observed measured $\delta^{13}C$ values, our model predicts that a 3-fold increase in productivity is required. Productivity alone seems unable to explain the recorded TOC mass accumulation rate values; preservation may play a key role. Phosphorus mass accumulation rates are in good agreement with the model results, suggesting that this element is associated first with productivity and then with preservation. The initial increase in productivity associated with the $\delta^{13}C$ excursion could be explained by the complex interaction of sea level rise, CO_2 release from volcanic provinces, and remobilization of nutrients in the oceans. However, our data do not provide any insights into this. The increased accumulation of organic matter and depletion of oxygen in the water column may have led to enhanced preservation of organic carbon. In the future an attempt to incorporate additional factors into the model, such as the local palaeoenvironmental situation, should be made. The model also needs to be tested in different environmental settings. The ISOAE model results show promise as a tool for testing ideas regarding productivity-driven accumulation of organic matter. The model could be improved significantly by using other concepts, such as diffusion, as well as incorporating a better understanding of Cretaceous ocean-water chemistry.

Acknowledgements

We would like to thank Michèle Caron for training in foraminiferid determination, Gesine Preuss for stable isotope laboratory assistance, P. Ducommun for geochemical analysis on the Manilva Section, André Villard for thin section preparation, G. Paratte, S. Affolter and F. Tamburini for helping to collect the samples and R. Coccioni, A. Martin-Algarra and L. O'Dogherty for introducing us to the Furlo and Manilva Sections. We thank G. Keller for constructive comments, Valeria Luciani and Silke Voigt for helpful reviews which greatly benefited this manuscript. We also thank Chris Wood for editorial comments. This study was supported by FNRS No: 21-67702.02.

References

Abdallah, H., Meister, C., 1997. The Cenomanian-Turonian boundary in the Gafsa-Chott area (southern part of central Tunisia): biostratigraphy, palaeoenvironments. Cretaceous Research 18, 197−236.

Accarie, H., Emmanuel, L., Robaszynski, F., Baudin, F., Amedro, F., Caron, M., Deconinck, J.F., 1996. Carbon isotope geochemistry (delta C-13) as stratigraphic tool. A case study of the Cenomanian/Turonian boundary in central Tunisia. Comptes Rendus de l'Académie des Sciences − Series IIA − Earth and Planetary Science 322, 579−586.

Adatte, T., Stinnesbeck, W., Keller, G., 1996. Lithostratigraphical and mineralogic correlations of near K/T boundary clastic sediments in northeastern Mexico: implications for origin and nature of deposition. Geological Society of America Special Paper 307, 211−226.

Arthur, M., Premoli-Silva, I., 1982. Development of widespread organic rich strata in Mediterranean Tethys. In: Schlanger, A., Cita, M.B. (Eds.), Nature and Origin of Cretaceous Carbon-rich Facies. Academic Press, London/New York/Paris, pp. 7−54.

Attewell, P.B., Farmer, I.W., 1976. Principles of Engineering Geology. Chapman and Hall, London.

Beaudoin, B., M'Ban, E.P., Montanari, A., Pinault, M., 1996. Stratigraphie haute résolution (<20 ka) dans le Cénomanien du bassin de Marches-Ombrie (Italie). (High-resolution lithostratigraphy in the Cenomanian of

the Umbria-Marche Basin (Italy)). Comptes Rendus de l'Académie des Sciences 323, 689−696.

Bortolotti, V., Passerini, P., Sagri, M., Sestini, G., 1970. The miogeosynclinal sequences. Sedimentary Geology 4, 341−344.

Bralower, T.J., Thierstein, H.R., 1984. Low productivity and slow deep-water circulation in the mid-Cretaceous oceans. Geology 4, 341−444.

Buchbinder, B., Benjamini, C., Lipson-Benitah, S., 2000. Sequence development of Late Cenomanian−Turonian carbonate ramps, platforms and basins in Israel. Cretaceous Research 21, 813−843.

Caron, M., 1983. La spéciation chez les foraminifères planctiques: une réponse adaptée aux contraintes de l'environnement. Zitteliana 10, 671−676.

Caron, M., Robaszynski, F., Amedro, F., Baudin, F., Deconinck, J.F., Hochuli, P., Salis-Perche Neilsen, K.V., Tribovillard, N., 1999. Estimation de la durée de l'événement anoxique global au passage Cénomanien/Turonien. Approche cyclostratigraphique dans la formation Bahloul en Tunisie centrale. Bulletin de la Société Géologique de France 170, 145−160.

Coccioni, R., Erba, E., Premoli-Silva, I., 1991. Litho- and bisotratigraphy of the Livello Bonarelli close to the Cenomanian/Turonian boundary (Umbria-Marche Apennines, Italy) and possible paleoceanographic significance. Géologie Alpine, Mémoire Hors Série 17, 25−26.

Cresta, S., Monechi, S., Parisi, G., Baldamza, A., Reale, V., 1989. Mesozoic−Cenozoic stratigraphy in the Umbria-Marche area. Memoria Cartagraphica Geologia de Italia 39, 185.

Crumiere, J.P., Crumiereairaud, C., Espitalie, J., 1990. Cyclic preservation of amorphous organic-matter in sediments of the Vocontian Basin (Southeastern France), around the Cenomanian−Turonian boundary − paleoceanographic controls. Bulletin de la Société Géologique de France 6, 469−478.

Davey, S.D., Jenkyns, H.C., 1999. Carbon-isotope stratigraphy of shallow-water limestones and implications for the timing of Late Cretaceous sea-level rise and anoxic events (Cenomanian−Turonian of the peri-Adriatic carbonate platform, Croatia). Eclogae Geologicae Helvetiae 92, 163−170.

Demaison, G.T., Moore, G.T., 1980. Anoxic environments and oil source bed genesis. Organic Geochemistry 2, 9−31.

Eaton, A.D., Clesceri, L.S., Greenberg, A.E., 1995. Standard Methods for the Examination of Water and Wastewater. American Public Health Association, New York.

Elder, W.P., Kirkland, J.I., 1985. Statigraphy and depositional environment of the Bridge Creek Limestone Member of the Greenhorn Formation at Rock Canyon Anticline near Pueblo, Colorado. In: Fine Grained Deposits and Biofacies of the Cretaceous Western Interior Seaway: Evidence of Cyclic Sedimentary Processes. Field Trip Guidebook, vol. 4. Society of Economic Paleontologists and Mineralogists, Tulsa.

Espitalié, J., Deroo, G., Marquis, F., 1985. La pyrolyse Rock-Eval et ses applications. Revue de l'Institut Français du Pétrole 40, 563−579.

Ferrandini, M., Philip, J., Babinot, J.F., Ferrandini, J., Tronchetti, G., 1985. The Cenomanian−Turonian carbonate platform in the Erfoud-Errachidia area (Southeastern Morocco) − stratigraphy and paleoenvironments. Bulletin de la Société Géologique de France 1, 559−564.

Föllmi, K.B., 1996. The phosphorus cycle, phosphogenesis and marine phosphate-rich deposits. Earth-Science Reviews 40, 55−124.

Gale, A.S., Jenkyns, H.C., Kennedy, W.J., Corfield, R.M., 1993. Chemostratigraphy versus biostratigraphy − data from around the Cenomanian−Turonian boundary. Journal of the Geological Society 150, 29−32.

Hardenbol, J., Thierry, J., Farley, M.B., Jacquin, T., De Graciansky, P.-C., Vail, P.R., 1998. Mesozoic and Cenozoic sequence chronostrigraphic framework of European Basins. In: Graciansky, J., Hardenbol, T. (Eds.), Mesozoic and Cenozoic Sequence Stratigraphy of European Basins. Society of Economic Paleontologists and Mineralogists Special Publication, vol. 60, pp. 3−13.

Jenkyns, H.C., 1980. Cretaceous anoxic events, from continents to oceans. Journal of the Geological Society of London 137, 171−188.

Kauffman, E.G., 1995. Global Change Leading to Biodiversity Crisis in a Greenhouse World: The Cenomanian−Turonian (Cretaceous) Mass Extinction, Effects of Global Change on Life. Panel on Effects of Past Global Change on Life. National Research Council, pp. 47−71.

Keller, G., Han, Q., Adatte, T., Burns, S.J., 2001. Palaeoenvironment of the Cenomanian−Turonian transition at Eastbourne, England. Cretaceous Research 22, 391−422.

Keller, G., Pardo, A., 2004. Age and paleoenvironment of the Cenomanian−Turonian global stratotype section and point at Pueblo, Colorado. Marine Micropalaeontology 51, 95−128.

Keller, G., Stueben, D., Berner, Z., Adatte, T., 2004. Cenomanian−Turonian d13C, d18O, sea level and salinity variations at Pueblo, Colorado. Palaeogeography, Palaeoclimatology, Palaeoecology 211, 19−43.

Kolonic, S., Damste, J.S.S., Bottcher, M.E., Kuypers, M.M.M., Kuhnt, W., Beckmann, B., Scheeder, G., Wagner, T., 2002. Geochemical characterization of Cenomanian/Turonian black shales from the Tarfaya Basin (SW Morocco) − relationships between palaeoenvironmental conditions and early sulphurization of sedimentary organic matter. Journal of Petroleum Geology 25, 325−350.

Kowallis, B.J., Christiansen, E.H., Deino, A.L., Kunk, M.J., Heaman, L.M., 1995. Age of the Cenomanian−Turonian boundary in the western interior of the United-States. Cretaceous Research 16, 109−129.

Kuhnt, W., Herbin, J.P., Thurow, J., Wiedmann, J., 1988. Cenomanian−Turonian organic facies in the western Mediterranean and along the adjacent Atlantic margin. American Association of Petroleum Geologists 72, 1011.

Kuhnt, W., Herbin, J.P., Thurow, J., Wiedmann, J., 1990. Distribution of Cenomanian−Turonian oragnic facies in the western Mediterranean and along the adjacent Atlantic margin. In: Huc, A.Y. (Ed.), Deposition of Organic Facies. AAPG Studies in Geology, vol. 30, pp. 133−160.

Kübler, B., 1987. Cristallinite de l'illite, méthods normalisées de préparations, méthodes normalisées de mesures. Cahier Insitut de Géologie, Série ADX 1, 1−13.

Lamolda, M.A., Gorostidi, A., Paul, C.R.C., 1994. Quantitative estimates of Calcareous Nannofossil changes across the Plenus Marls (Latest Cenomanian), Dover, England − implications for the generation of the Cenomanian−Turonian boundary event. Cretaceous Research 15, 143−164.

Larson, R.L., 1991. Geoogical consequences of superplumes. Geology 19, 963−966.

Larson, R.L., Erba, E., 1999. Onset of the mid-Cretaceous greenhouse in the Barremian−Aptian: igneous events and the biological, sedimentary, and geochemical responses. Paleoceanography 14, 663−678.

Leckie, M.R., Bralower, T.J., Cashman, R., 2002. Oceanic anoxic events and plankton evolution: biotic response to tectonic forcing during the mid-Cretaceous. Paleoceanography 17, 1−29.

Leckie, R.M., 1985. Foraminifera of the Cenomanian−Turonian boundary interval, Greenhorn Formation, Rock Canyon Anticline, Pueblo, Colorado. In: Pratt, L.M., Kauffman, E.G., Zelt, F.B. (Eds.), Fine-grained Deposits and Biofacies of the Cretaceous Western interior Seaway: Evidence of Cyclic Sedimentary Processes. Field Trip Guidebook No. 4. Society of Economic Paleontologists and Mineralogists. Tulsa, pp. 139−149.

Leckie, R.M., 1987. Paleoecology of mid-Cretaceous planktic foraminifera: a comparison of open ocean and epicontinental sea assemblages. Micropaleontology 33, 164−176.

Martinez, P.H., Bertrand, P.H., Bouloubassi, I., Bareille, G., et al., 1996. An integrated view of inorganic and organic biogeochemical indicators of palaeoproductivity changes in a coastal upwelling area. Organic Geochemistry 24, 411−420.

McArthur, R.H., Wilson, E.O., 1967. The Theory of Island Biogeography. Princeton University Press.

Mermighis, A., Philip, J., Tronchetti, G., 1991. Carbonate platform sequences and system tracts at the Cenomanian−Turonian boundary, internal Hellenids (Peloponnesus, Greece). Bulletin de la Société Géologique de France 162, 547−552.

Meyers, S., Sageman, B.B., 2004. Detection, quatification and significance of hiatuses in pelagic and hemipelagic strata. Earth and Planetary Science Letters 224, 55−72.

Meyers, S.R., Sageman, B.B., Hinnov, L.A., 2001. Integrated quantitative stratigraphy of the Cenomanian−Turonian bridge creek limestone member using evolutive harmonic analysis and stratigraphic modeling. Journal of Sedimentary Research 71, 628−644.

Mort, H.P., Adatte, T., Keller, G., Föllmi, K.B., Steinmann, P., Matera, V., Berner, Z., Stuben, D., 2007. Phosphorus and the roles of productivity

and nutrient recycling during Oceanic Anoxic Event 2. Geology 35 (6), 483−486.

Nederbragt, A.J., Fiorentino, A., 1999. Stratigraphy and palaeoceanography of the Cenomanian−Turonian boundary event in Oued Mellegue, northwestern Tunisia. Cretaceous Research 20, 47−62.

Obradovitch, J.D., 1993. A Cretaceous timescale. In: Caldwell, W.G.E., Kauffman, E.G. (Eds.), Evolution of the Western Interior Basin. Geological Association of Canada Special Paper, pp. 47−62.

Paul, C.R.C., Larnolda, M.A., Mitchell, S.F., Vaziri, M.R., Gorostidi, A., 1999. The Cenomanian−Turonian boundary at Eastbourne (Sussex, UK): a proposed European reference section. Palaeogeography, Palaeoclimatology, Palaeoecology 150, 83−121.

Pedersen, T.F., Calvert, S.E., 1990. Anoxia vs. productivity: what controls the formation of organic carbon-rich sediments and sedimentary rocks? Bulletin of the American Association of Petroleum Geologists 74, 454−466.

Pratt, L.M., 1985. Isotopic studies of organic matter and carbonate in rocks of the Greenhorn marine cycles. In: Pratt, L.A., Kauffman, E.G., Zelt, F.B. (Eds.), Fine Grained Deposits and Biofacies of the Cretaceous Western Interior Seaway: Evidence of Cyclic Sedimentary Processes. Field Trip Guidebook, vol. 4. Society of Economic Paleotologists and Mineralogists, Tulsa, pp. 38−48.

Pratt, L.M., Arthur, M.A., Dean, W.E., Scholle, P.A., 1993. Paleoceanographic cycles and events during the late Cretaceous in the western interior seaway of North America. In: Caldwell, M.W., Kauffman, E.G. (Eds.), Evolution of the Western Interior Basin. St John's Geological Association of Canada Special Paper, vol. 39, pp. 333−354.

Premoli-Silva, I., Erba, E., Salvini, G., Locatelli, C., Verga, D., 1999. Biotic changes in Cretcaeous oceanic anoxic events of the Tethys. Journal of Foraminiferal Research 29, 352.

Reicherter, K., Pletsch, T., Kuhnt, W., Manthey, J., Homeier, G., Wiedmann, J., Thurow, J., 1994. Mid-Cretaceous paleogeography and paleoceanography of the Betic Seaway (Betic Cordillera, Spain). Palaeogeography, Palaeoclimatology, Palaeoecology 107, 1−33.

Ryan, W.B.F., Cita, M.B., 1977. Ignorance concerning episodes of ocean-wide stagnation. Marine Geology 23, 197−215.

Sageman, B.B., Meyers, S.R., Arthur, M.A., 2006. Orbital time scale and new C-isotope record for the Cenomanian−Turonion boundary stratotyoe. Geology 34 (2), 125−128.

Sageman, B.B., Rich, J., Arthur, M.A., Dean, W.E., Savrda, C.E., Bralower, T.J., 1998. Multiple Milankovich cycles in the Bridge Creek Limestone (Cenomanian−Turonian), western interior basin. In: Dean, W.E., Arthur, M.A. (Eds.), Concepts in Sedimentology and Paleontology. Society for Sedimentary Geology, vol. 6, pp. 153−171.

Sarmiento, J.L., Dunne, J., Gnanadesikan, R.M., Matsumoto, K., Slater, R., 2002. A new estimate of the CaCO3 to organic carbon export ratio. Global Biogeochemical Cycles 16, 1−12.

Schlanger, S.O., Arthur, M.A., Jenkyns, H.C., Scholle, P.A., 1987. The Cenomanian/Turonian anoxic event deposits. In: Einsele, G., Seilacher, A. (Eds.), Cyclic and Event Stratification. Springer-Verlag, New York, pp. 161−173.

Schlanger, S.O., Jenkyns, H.C., 1976. Cretaceous oceanic anoxic events: causes and consequences. Geologie en Mijnbouw 55, 179−184.

Schlanger, S.O., Jenkyns, H.C., Premoli-silva, I., 1981. Volcanism and vertical Tectonics in the Pacific Basin related to global Cretaceous trangressions. Earth and Planetary Science Letters 52, 435−449.

Scholle, P.A., Arthur, M.A., 1980. Carbon isotope fluctuations in Cretaceous pelagic limestones: potential stratigraphic and petroleum exploration tool. Bulletin American Association of Petroleum Geologists 64, 67−87.

Scott, R.W., Evetts, M.J., Franks, P.C., Bergen, J.A., Stein, J.A., 1998. Timing of mid-Cretaceous relative sea level changes in the western interior: Amoco No. 1 Bounds Core. In: Dean, W.E., Arthur, M.A. (Eds.), SEPM Concepts in Sedimentology and Paleontology, vol. 6, pp. 11−34.

Shimkus, K., Trimonis, E., 1974. Modern sedimentation in the Black sea. In: Degens, E.T., Ross, D.A. (Eds.), The Black Sea-Geology, Chemistry and Biology. American Association of Petroleum Geologists Memoir, vol. 20, pp. 249−278.

Siegenthaler, U., Sarmiento, J.L., 1980. Atmospheric carbon dioxide and the ocean. Nature 365, 119−125.

Snow, L.J., Duncan, R.A., Bralower, T.J., 2005. Trace element abundance in the Rock Canyon Anticline, Pueblo, Colorado, marine sedimentary section and their relationship to Caribbean plateau construction and oxygen anoxic event 2. Paleoceanography 20, doi:10.1029/2004PA001093.

Thurow, J., Moullade, M., Brumsack, H.J., Masure, E., Taugourdeau-Lantz, J., 1988. The Cenomanian/Turonian boundary event (CTBE) at hole 641A, ODP Leg 103 (compared with CTBE interval at site 398). The Proceedings of the Ocean Drilling Program, Scientific Results 103, 587−634.

Tissot, B.P., Welte, D., 1984. Petroleum Formation and Occurrence. Chapmand and Hall, London, 699 pp.

Tsikos, H., Jenkyns, H.C., Walsworth-Bell, B., Petrizzo, M.R., et al., 2004. Carbon-isotope stratigraphy recorded by the Cenomanian−Turonian oceanic anoxic event: correlation and implications based on three key localities. Journal of the Geological Society 161, 711−719.

Weissert, H., Lini, A., Kuhnt, O., 1998. Correlation of Early Cretaceous carbon isotope stratigraphy and platform drowning events: a possible link? Palaeogeography, Palaeoclimatology, Palaeoecology 137, 89−203.